Observation of $e^+e^- \to \pi^0\pi^0 h_c$ and a neutral charmoniumlike structure $Z_c(4020)^0$

M. Ablikim[1], M. N. Achasov[8,a], X. C. Ai[1], O. Albayrak[4], M. Albrecht[3], D. J. Ambrose[42], A. Amoroso[46A,46C], F. F. An[1], Q. An[43], J. Z. Bai[1], R. Baldini Ferroli[19A], Y. Ban[30], D. W. Bennett[18], J. V. Bennett[4], M. Bertani[19A], D. Bettoni[20A], J. M. Bian[41], F. Bianchi[46A,46C], E. Boger[22,g], O. Bondarenko[24], I. Boyko[22], R. A. Briere[4], H. Cai[48], X. Cai[1], O. Cakir[38A], A. Calcaterra[19A], G. F. Cao[1], S. A. Cetin[38B], J. F. Chang[1], G. Chelkov[22,b], G. Chen[1], H. S. Chen[1], H. Y. Chen[2], J. C. Chen[1], M. L. Chen[1], S. J. Chen[28], X. Chen[1], X. R. Chen[25], Y. B. Chen[1], H. P. Cheng[16], X. K. Chu[30], Y. P. Chu[1], G. Cibinetto[20A], D. Cronin-Hennessy[41], H. L. Dai[1], J. P. Dai[1], D. Dedovich[22], Z. Y. Deng[1], A. Denig[21], I. Denysenko[22], M. Destefanis[46A,46C], F. De Mori[46A,46C], Y. Ding[26], C. Dong[29], J. Dong[1], L. Y. Dong[1], M. Y. Dong[1], S. X. Du[50], P. F. Duan[1], J. Z. Fan[37], J. Fang[1], S. S. Fang[1], X. Fang[43], Y. Fang[1], L. Fava[46B,46C], F. Feldbauer[21], G. Felici[19A], C. Q. Feng[43], E. Fioravanti[20A], C. D. Fu[1], Q. Gao[1], Y. Gao[37], I. Garzia[20A], K. Goetzen[9], W. X. Gong[1], W. Gradl[21], M. Greco[46A,46C], M. H. Gu[1], Y. T. Gu[11], Y. H. Guan[1], A. Q. Guo[1], L. B. Guo[27], T. Guo[27], Y. Guo[1], Y. P. Guo[21], Z. Haddadi[24], A. Hafner[21], S. Han[48], Y. L. Han[1], F. A. Harris[40], K. L. He[1], Z. Y. He[29], T. Held[3], Y. K. Heng[1], Z. L. Hou[1], C. Hu[27], H. M. Hu[1], J. F. Hu[46A], T. Hu[1], Y. Hu[1], G. M. Huang[5], G. S. Huang[43], H. P. Huang[48], J. S. Huang[14], X. T. Huang[32], Y. Huang[28], T. Hussain[45], Q. Ji[1], Q. P. Ji[29], X. B. Ji[1], X. L. Ji[1], L. L. Jiang[1], L. W. Jiang[48], X. S. Jiang[1], J. B. Jiao[32], Z. Jiao[16], D. P. Jin[1], S. Jin[1], T. Johansson[47], A. Julin[41], N. Kalantar-Nayestanaki[24], X. L. Kang[1], X. S. Kang[29], M. Kavatsyuk[24], B. C. Ke[4], R. Kliemt[13], B. Kloss[21], O. B. Kolcu[38B,c], B. Kopf[3], M. Kornicer[40], W. Kuehn[23], A. Kupsc[47], W. Lai[1], J. S. Lange[23], M. Lara[18], P. Larin[13], M. Leyhe[3], Cheng Li[43], D. M. Li[50], F. Li[1], G. Li[1], H. B. Li[1], J. C. Li[1], Jin Li[31], K. Li[12], K. Li[32], Q. J. Li[1], T. Li[32], W. D. Li[1], W. G. Li[1], X. L. Li[32], X. M. Li[11], X. N. Li[1], X. Q. Li[29], Z. B. Li[36], H. Liang[43], Y. F. Liang[34], Y. T. Liang[23], G. R. Liao[10], D. X. Lin[13], B. J. Liu[1], C. L. Liu[4], C. X. Liu[1], F. H. Liu[33], Fang Liu[1], Feng Liu[5], H. B. Liu[11], H. H. Liu[1], H. H. Liu[15], H. M. Liu[1], J. Liu[1], J. P. Liu[48], J. Y. Liu[1], K. Liu[37], K. Y. Liu[26], L. D. Liu[30], Q. Liu[39], S. B. Liu[43], X. Liu[25], X. X. Liu[39], Y. B. Liu[29], Z. A. Liu[1], Zhiqiang Liu[1], Zhiqing Liu[21], H. Loehner[24], X. C. Lou[1,d], H. J. Lu[16], J. G. Lu[1], R. Q. Lu[17], Y. Lu[1], Y. P. Lu[1], C. L. Luo[27], M. X. Luo[49], T. Luo[40], X. L. Luo[1], M. Lv[1], X. R. Lyu[39], F. C. Ma[26], H. L. Ma[1], Q. M. Ma[1], S. Ma[1], T. Ma[1], X. N. Ma[29], X. Y. Ma[1], F. E. Maas[13], M. Maggiora[46A,46C], Q. A. Malik[45], Y. J. Mao[30], Z. P. Mao[1], S. Marcello[46A,46C], J. G. Messchendorp[24], J. Min[1], T. J. Min[1], R. E. Mitchell[18], X. H. Mo[1], Y. J. Mo[5], H. Moeini[24], C. Morales Morales[13], K. Moriya[18], N. Yu. Muchnoi[8,a], H. Muramatsu[41], Y. Nefedov[22], F. Nerling[13], I. B. Nikolaev[8,a], Z. Ning[1], S. Nisar[7], S. L. Niu[1], X. Y. Niu[1], S. L. Olsen[31], Q. Ouyang[1], S. Pacetti[19B], P. Patteri[19A], M. Pelizaeus[3], H. P. Peng[43], K. Peters[9], J. L. Ping[27], R. G. Ping[1], R. Poling[41], Y. N. Pu[17], M. Qi[28], S. Qian[1], C. F. Qiao[39], L. Q. Qin[32], N. Qin[48], X. S. Qin[1], Y. Qin[30], Z. H. Qin[1], J. F. Qiu[1], K. H. Rashid[45], C. F. Redmer[21], H. L. Ren[17], M. Ripka[21], G. Rong[1], X. D. Ruan[11], V. Santoro[20A], A. Sarantsev[22,e], M. Savrié[20B], K. Schoenning[47], S. Schumann[21], W. Shan[30], M. Shao[43], C. P. Shen[2], P. X. Shen[29], X. Y. Shen[1], H. Y. Sheng[1], M. R. Shepherd[18], W. M. Song[1], X. Y. Song[1], S. Sosio[46A,46C], S. Spataro[46A,46C], B. Spruck[23], G. X. Sun[1], J. F. Sun[14], S. S. Sun[1], Y. J. Sun[43], Y. Z. Sun[1], Z. J. Sun[1], C. J. Tang[34], X. Tang[1], I. Tapan[38C], E. H. Thorndike[42], M. Tiemens[24], D. Toth[41], M. Ullrich[23], I. Uman[38B], G. S. Varner[40], B. Wang[29], B. L. Wang[39], D. Wang[30], D. Y. Wang[30], K. Wang[1], L. L. Wang[1], L. S. Wang[1], M. Wang[32], P. Wang[1], P. L. Wang[1], Q. J. Wang[1], S. G. Wang[30], W. Wang[1], X. F. Wang[37], Y. F. Wang[1], Y. Q. Wang[21], Z. Wang[1], Z. G. Wang[1], Z. H. Wang[43], Z. Y. Wang[1], D. H. Wei[10], J. B. Wei[30], P. Weidenkaff[21], S. P. Wen[1], U. Wiedner[3], M. Wolke[47], L. H. Wu[1], Z. Wu[1], L. G. Xia[37], Y. Xia[17], D. Xiao[1], Z. J. Xiao[27], Y. G. Xie[1], Q. L. Xiu[1], G. F. Xu[1], L. Xu[1], Q. J. Xu[12], Q. N. Xu[39], X. P. Xu[35], Z. Xue[1], L. Yan[43], W. B. Yan[43], W. C. Yan[43], Y. H. Yan[17], H. X. Yang[1], L. Yang[48], Y. Yang[5], Y. X. Yang[10], H. Ye[1], M. Ye[1], M. H. Ye[6], J. H. Yin[1], B. X. Yu[1], C. X. Yu[29], H. W. Yu[30], J. S. Yu[25], C. Z. Yuan[1], W. L. Yuan[28], Y. Yuan[1], A. Yuncu[38B,f], A. A. Zafar[45], A. Zallo[19A], Y. Zeng[17], B. X. Zhang[1], B. Y. Zhang[1], C. Zhang[28], C. C. Zhang[1], D. H. Zhang[1], H. H. Zhang[36], H. T. Zhang[1], H. Y. Zhang[1], J. J. Zhang[1], J. L. Zhang[1], J. Q. Zhang[1], J. W. Zhang[1], J. Y. Zhang[1], J. Z. Zhang[1], K. Zhang[1], L. Zhang[1], S. H. Zhang[1], X. J. Zhang[1], X. Y. Zhang[32], Y. Zhang[1], Y. H. Zhang[1], Z. H. Zhang[5], Z. P. Zhang[43], Z. Y. Zhang[48], G. Zhao[1], J. W. Zhao[1], J. Y. Zhao[1], J. Z. Zhao[1], Lei Zhao[43], Ling Zhao[1], M. G. Zhao[29], Q. Zhao[1], Q. W. Zhao[1], S. J. Zhao[50], T. C. Zhao[1], Y. B. Zhao[1], Z. G. Zhao[43], A. Zhemchugov[22,g], B. Zheng[44], J. P. Zheng[1], Y. H. Zheng[39], B. Zhong[27], L. Zhou[1], Li Zhou[29], X. Zhou[48], X. K. Zhou[43], X. R. Zhou[43], X. Y. Zhou[1], K. Zhu[1], K. J. Zhu[1], S. Zhu[1], X. L. Zhu[37], Y. C. Zhu[43], Y. S. Zhu[1], Z. A. Zhu[1], J. Zhuang[1], B. S. Zou[1], J. H. Zou[1]

(BESIII Collaboration)

[1] *Institute of High Energy Physics, Beijing 100049, People's Republic of China*
[2] *Beihang University, Beijing 100191, People's Republic of China*
[3] *Bochum Ruhr-University, D-44780 Bochum, Germany*
[4] *Carnegie Mellon University, Pittsburgh, Pennsylvania 15213, USA*
[5] *Central China Normal University, Wuhan 430079, People's Republic of China*
[6] *China Center of Advanced Science and Technology, Beijing 100190, People's Republic of China*
[7] *COMSATS Institute of Information Technology, Lahore, Defence Road, Off Raiwind Road, 54000 Lahore, Pakistan*
[8] *G.I. Budker Institute of Nuclear Physics SB RAS (BINP), Novosibirsk 630090, Russia*
[9] *GSI Helmholtzcentre for Heavy Ion Research GmbH, D-64291 Darmstadt, Germany*
[10] *Guangxi Normal University, Guilin 541004, People's Republic of China*
[11] *GuangXi University, Nanning 530004, People's Republic of China*
[12] *Hangzhou Normal University, Hangzhou 310036, People's Republic of China*
[13] *Helmholtz Institute Mainz, Johann-Joachim-Becher-Weg 45, D-55099 Mainz, Germany*
[14] *Henan Normal University, Xinxiang 453007, People's Republic of China*
[15] *Henan University of Science and Technology, Luoyang 471003, People's Republic of China*

[16] *Huangshan College, Huangshan 245000, People's Republic of China*
[17] *Hunan University, Changsha 410082, People's Republic of China*
[18] *Indiana University, Bloomington, Indiana 47405, USA*
[19] *(A)INFN Laboratori Nazionali di Frascati, I-00044, Frascati, Italy; (B)INFN and University of Perugia, I-06100, Perugia, Italy*
[20] *(A)INFN Sezione di Ferrara, I-44122, Ferrara, Italy; (B)University of Ferrara, I-44122, Ferrara, Italy*
[21] *Johannes Gutenberg University of Mainz, Johann-Joachim-Becher-Weg 45, D-55099 Mainz, Germany*
[22] *Joint Institute for Nuclear Research, 141980 Dubna, Moscow region, Russia*
[23] *Justus Liebig University Giessen, II. Physikalisches Institut, Heinrich-Buff-Ring 16, D-35392 Giessen, Germany*
[24] *KVI-CART, University of Groningen, NL-9747 AA Groningen, The Netherlands*
[25] *Lanzhou University, Lanzhou 730000, People's Republic of China*
[26] *Liaoning University, Shenyang 110036, People's Republic of China*
[27] *Nanjing Normal University, Nanjing 210023, People's Republic of China*
[28] *Nanjing University, Nanjing 210093, People's Republic of China*
[29] *Nankai University, Tianjin 300071, People's Republic of China*
[30] *Peking University, Beijing 100871, People's Republic of China*
[31] *Seoul National University, Seoul, 151-747 Korea*
[32] *Shandong University, Jinan 250100, People's Republic of China*
[33] *Shanxi University, Taiyuan 030006, People's Republic of China*
[34] *Sichuan University, Chengdu 610064, People's Republic of China*
[35] *Soochow University, Suzhou 215006, People's Republic of China*
[36] *Sun Yat-Sen University, Guangzhou 510275, People's Republic of China*
[37] *Tsinghua University, Beijing 100084, People's Republic of China*
[38] *(A)Ankara University, Dogol Caddesi, 06100 Tandogan, Ankara, Turkey; (B)Dogus University, 34722 Istanbul, Turkey; (C)Uludag University, 16059 Bursa, Turkey*
[39] *University of Chinese Academy of Sciences, Beijing 100049, People's Republic of China*
[40] *University of Hawaii, Honolulu, Hawaii 96822, USA*
[41] *University of Minnesota, Minneapolis, Minnesota 55455, USA*
[42] *University of Rochester, Rochester, New York 14627, USA*
[43] *University of Science and Technology of China, Hefei 230026, People's Republic of China*
[44] *University of South China, Hengyang 421001, People's Republic of China*
[45] *University of the Punjab, Lahore-54590, Pakistan*
[46] *(A)University of Turin, I-10125, Turin, Italy; (B)University of Eastern Piedmont, I-15121, Alessandria, Italy; (C)INFN, I-10125, Turin, Italy*
[47] *Uppsala University, Box 516, SE-75120 Uppsala, Sweden*
[48] *Wuhan University, Wuhan 430072, People's Republic of China*
[49] *Zhejiang University, Hangzhou 310027, People's Republic of China*
[50] *Zhengzhou University, Zhengzhou 450001, People's Republic of China*

[a] *Also at the Novosibirsk State University, Novosibirsk, 630090, Russia*
[b] *Also at the Moscow Institute of Physics and Technology, Moscow 141700, Russia and at the Functional Electronics Laboratory, Tomsk State University, Tomsk, 634050, Russia*
[c] *Currently at Istanbul Arel University, Kucukcekmece, Istanbul, Turkey*
[d] *Also at University of Texas at Dallas, Richardson, Texas 75083, USA*
[e] *Also at the PNPI, Gatchina 188300, Russia*
[f] *Also at Bogazici University, 34342 Istanbul, Turkey*
[g] *Also at the Moscow Institute of Physics and Technology, Moscow 141700, Russia*

Using data collected with the BESIII detector operating at the Beijing Electron Positron Collider at center-of-mass energies of $\sqrt{s} = 4.23$, 4.26, and 4.36 GeV, we observe $e^+e^- \to \pi^0\pi^0 h_c$ for the first time. The Born cross sections are measured and found to be about half of those of $e^+e^- \to \pi^+\pi^- h_c$ within less than 2σ. In the $\pi^0 h_c$ mass spectrum, a structure at 4.02 GeV/c^2 that is most likely the neutral isospin partner of the $Z_c(4020)^\pm$ observed in the process of $e^+e^- \to \pi^+\pi^- h_c$ is found. A fit to the $\pi^0 h_c$ invariant mass spectrum with the width of the $Z_c(4020)^0$ fixed to that of its charged isospin partner and possible interferences with non-$Z_c(4020)^0$ amplitudes neglected, gives a mass of $(4023.9 \pm 2.2 \pm 3.8)$ MeV/c^2 for the $Z_c(4020)^0$, where the first error is statistical and the second systematic.

PACS numbers: 14.40.Rt, 13.66.Bc, 14.40.Pq

In the study of $e^+e^- \to \pi^+\pi^- J/\psi$, a distinct charged structure, $Z_c(3900)^\pm$, was observed in the $\pi^\pm J/\psi$ spec-

trum by the BESIII [1] and Belle [2] experiments, and confirmed shortly thereafter with CLEO-c data [3]. A similar charged structure but with a slightly higher mass, $Z_c(4020)^{\pm}$, was soon reported in $e^+e^- \to \pi^+\pi^- h_c$ [4] by BESIII. As there are at least four quarks within these two charmoniumlike structures, they are interpreted as either tetraquark states, $D\bar{D}^*$ molecules, hadrocharmonia, or other configurations [8]. More recently, charged structures in the same mass region were observed via their decays into charmed meson pairs, including the charged $Z_c(4025)^{\pm}$ in $e^+e^- \to \pi^{\pm}(D^*\bar{D}^*)^{\mp}$ [9] and the charged $Z_c(3885)^{\pm}$ in $e^+e^- \to \pi^{\pm}(D\bar{D}^*)^{\mp}$ [10]. These structures together with the recently confirmed $Z(4430)^-$ [11–13] and similar structures observed in the bottomonium system [14] indicate that a new class of hadrons has been observed. An important question is whether all these charged structures are part of isospin $I = 1$ triplets, in which case neutral partners with $I_z = 0$ should also be found. Evidence for a neutral $Z_c(3900)$ was observed in $e^+e^- \to \pi^0\pi^0 J/\psi$ process with CLEO-C data at center-of-mass energy (CME) $\sqrt{s}$=4.17 GeV [3]. A neutral structure, the $Z_c(4020)^0$, is expected to couple to the $\pi^0 h_c$ final state and be produced for in $e^+e^- \to \pi^0\pi^0 h_c$ processes.

In this Letter, we present the first observation of $e^+e^- \to \pi^0\pi^0 h_c$ at $\sqrt{s} = 4.23$ GeV, 4.26 GeV, and 4.36 GeV, and the observation of a neutral charmoniumlike structure $Z_c(4020)^0$ in the $\pi^0 h_c$ spectrum. We follow closely the analysis of $e^+e^- \to \pi^+\pi^- h_c$ [4] with the selection of $\pi^+\pi^-$ replaced with the selection of a pair of π^0s. The data samples were collected with the BESIII detector [5]. The CMEs and corresponding integrated luminosities are listed in Table I.

We use a GEANT4 [6] based Monte Carlo (MC) simulation to optimize the event selection criteria, determine the detection efficiency, and estimate backgrounds. In the studies presented here, the h_c is reconstructed via its electric-dipole (E1) transition $h_c \to \gamma\eta_c$ with $\eta_c \to X_i$, where X_i denotes 16 hadronic final states: $p\bar{p}$, $\pi^+\pi^- K^+K^-$, $\pi^+\pi^- p\bar{p}$, $2(K^+K^-)$, $2(\pi^+\pi^-)$, $3(\pi^+\pi^-)$, $2(\pi^+\pi^-)K^+K^-$, $K_S K^{\pm}\pi^{\mp}$, $K_S K^{\pm}\pi^{\mp}\pi^+\pi^-$, $K^+K^-\pi^0$, $K^+K^-\eta$, $p\bar{p}\pi^0$, $\pi^+\pi^-\eta$, $\pi^+\pi^-\pi^0\pi^0$, $2(\pi^+\pi^-)\eta$, and $2(\pi^+\pi^-\pi^0)$. The initial state radiation (ISR) is simulated with KKMC [7], where the Born cross section of $e^+e^- \to \pi^0\pi^0 h_c$ is assumed to follow the $e^+e^- \to \pi^+\pi^- h_c$ line-shape [4].

The selection of charged tracks, photons, and $K_S^0 \to \pi^+\pi^-$ candidates are described in Refs. [4, 15]. A candidate π^0 (η) is reconstructed from a pair of photons with an invariant mass in the range $|M_{\gamma\gamma} - m_{\pi^0}| < 15$ MeV/c^2 ($|M_{\gamma\gamma} - m_{\eta}| < 15$ MeV/c^2), where m_{π^0} (m_{η}) is the nominal π^0 (η) mass [16]. The event candidates of $e^+e^- \to \pi^0\pi^0 h_c$, $h_c \to \gamma\eta_c$ are required to have at least one $\gamma\pi^0\pi^0$ combination with the mass recoiling against $\pi^0\pi^0$, $M_{\pi^0\pi^0}^{\text{recoil}}$, in the h_c mass region ($M_{\pi^0\pi^0}^{\text{recoil}} \in$ [3.3, 3.7] GeV/c^2) and with the mass recoiling against $\gamma\pi^0\pi^0$, $M_{\gamma\pi^0\pi^0}^{\text{recoil}}$, in the η_c mass region ($M_{\gamma\pi^0\pi^0}^{\text{recoil}} \in$ [2.8, 3.2] GeV/c^2).

To determine the species of final state particles and to select the best photon candidates when additional photons (and π^0 or η candidates) are found in an event, the combination with the minimum value of $\chi^2 = \chi_{4C}^2 + \Sigma_{i=1}^N \chi_{\text{PID}}^2(i) + \chi_{1C}^2$ is selected for further analysis. Here χ_{4C}^2 is the χ^2 of the initial-final four-momentum conservation (4C) kinematic fit, $\chi_{\text{PID}}^2(i)$ is the χ^2 of particle identification (PID) of each charged track using the energy loss in the main drift chamber and the time measured with the time-of-flight system, N is the number of the charged tracks, and χ_{1C}^2 is the sum of the 1C χ^2s of the π^0s and η in each final state with the mass of the daughter photons constrained to that of the parent. There is also a χ_{4C}^2 requirement, which is optimized by maximizing the figure of merit $S/\sqrt{S+B}$, where S and B are the numbers of Monte Carlo (MC) simulated signal and background events, respectively. The requirement $\chi_{4C}^2 < 30$ has an efficiency of 61% for η_c decays with only charged or K_S^0 particles in the final states, while the requirement $\chi_{4C}^2 < 25$ has an efficiency of 36% for the other decays [17]. A similar optimization is performed to determine the η_c candidate mass window around its nominal value, which is found to be ± 35 MeV/c^2 with an efficiency of 59% for η_c decays with only charged or K_S^0 particles in final states and 22% for the other decays.

The inset of Fig. 1 shows the scatter plot of $M_{\gamma\pi^0\pi^0}^{\text{recoil}}$, which corresponds to the invariant mass of the reconstructed η_c candidate, versus $M_{\pi^0\pi^0}^{\text{recoil}}$, which corresponds to the invariant mass of the reconstructed h_c candidate, summed over the events at $\sqrt{s} = 4.23$, 4.26, and 4.36 GeV, where a clear cluster of events corresponding to the $h_c \to \gamma\eta_c$ signal is observed. Figure 1 shows the projection of the invariant mass distribution of $\gamma\eta_c$ candidates for events in the η_c signal region ($M_{\gamma\pi^0\pi^0}^{\text{recoil}} \in$ [2.945, 3.015] GeV/c^2), where a clear peak at the h_c mass is observed. The events in the sideband regions, 2.865 GeV/$c^2 < M_{\gamma\pi^0\pi^0}^{\text{recoil}} < 2.900$ GeV/c^2 and 3.050 GeV/$c^2 < M_{\gamma\pi^0\pi^0}^{\text{recoil}} < 3.085$ GeV/c^2 are used to study the background. To extract the number of $\pi^0\pi^0 h_c$ signal events, the $M_{\pi^0\pi^0}^{\text{recoil}}$ mass spectrum is fitted with a MC simulated signal shape convolved with a Gaussian function to represent the data-MC mass resolution difference, together with a linear background term. A simultaneous fit to the $M_{\pi^0\pi^0}^{\text{recoil}}$ mass spectrum summed over the 16 η_c decay modes at the three CME points yields the numbers of $\pi^0\pi^0 h_c$ signal events ($n_{h_c}^{\text{obs}}$) listed in Table I. Figure 1 also shows the fit results summed over the three CME points.

The Born cross section $\sigma^B(e^+e^- \to \pi^0\pi^0 h_c)$ is calculated with the formula

$$\sigma^B(e^+e^- \to \pi^0\pi^0 h_c) =$$
$$\frac{n_{h_c}^{\text{obs}}}{\mathcal{L}(1+\delta^r)(1+\delta^v)\sum_{i=1}^{16}\epsilon_i \mathcal{B}(\eta_c \to X_i)\mathcal{B}(h_c \to \gamma\eta_c)}, \quad (1)$$

where $n_{h_c}^{\text{obs}}$ is the number of observed h_c signal events; $\mathcal{L}$ is the integrated luminosity; $(1 + \delta^r)$ is the initial radiative correction factor, which is taken to be the same

TABLE I. Energies ($\sqrt{s}$), luminosities ($\mathcal{L}$), numbers of events ($n_{h_c}^{\mathrm{obs}}$), average efficiencies ($\sum\limits_{i=1}^{16} \epsilon_i \mathcal{B}(\eta_c \to X_i)$), initial state radiative correction factor ($1+\delta^r$) [4], vacuum polarization factor ($1+\delta^v$), Born cross sections $\sigma^{\mathrm{B}}(e^+e^- \to \pi^0\pi^0 h_c)$ and ratios $\mathcal{R}_{\pi\pi h_c} = \frac{\sigma(e^+e^- \to \pi^0\pi^0 h_c)}{\sigma(e^+e^- \to \pi^+\pi^- h_c)}$, where the third errors are from the uncertainty in $\mathcal{B}(h_c \to \gamma\eta_c)$ [20].

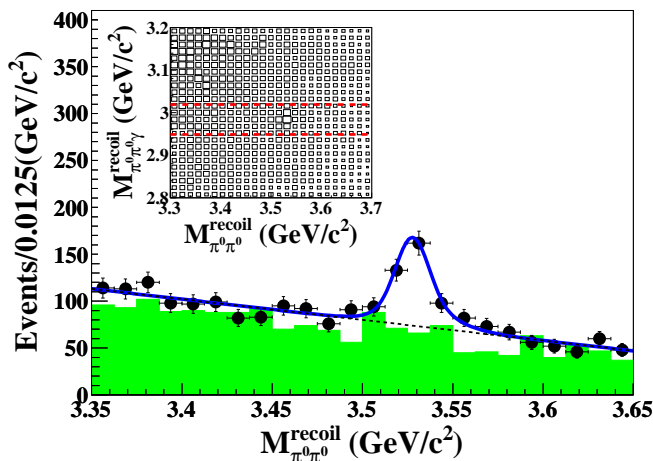| $\sqrt{s}$ (GeV)	$\mathcal{L}$ (pb^{-1})	$n_{h_c}^{\mathrm{obs}}$	$\sum\limits_{i=1}^{16} \epsilon_i \mathcal{B}(\eta_c \to X_i)$	$1+\delta^r$	$1+\delta^v$	$\sigma^{\mathrm{B}}(e^+e^- \to \pi^0\pi^0 h_c)$ (pb)	$\mathcal{R}_{\pi\pi h_c}$
4.230	1090.0	82.5 ± 15.6	6.82×10^{-3}	0.756	1.056	$25.6 \pm 4.8 \pm 2.6 \pm 4.0$	$0.54 \pm 0.11 \pm 0.06$
4.260	826.8	62.8 ± 13.3	6.54×10^{-3}	0.831	1.054	$24.4 \pm 5.2 \pm 3.2 \pm 3.8$	$0.63 \pm 0.14 \pm 0.10$
4.360	544.5	64.3 ± 11.5	6.68×10^{-3}	0.856	1.051	$36.2 \pm 6.5 \pm 4.1 \pm 5.7$	$0.73 \pm 0.14 \pm 0.10$

FIG. 1. The $M_{\pi^0\pi^0}^{\mathrm{recoil}}$ distribution for the events with an η_c candidate. The plot shows the sum over three CME points. Dots with error bars are data; the solid curve is the best fit; the dashed black line is the background; the green shaded histogram shows the normalized η_c sideband events. The inset shows the scatter plot of $M_{\gamma\pi^0\pi^0}^{\mathrm{recoil}}$ versus $M_{\pi^0\pi^0}^{\mathrm{recoil}}$. The two red dashed lines represent the signal region of η_c.

as that for the analysis of $e^+e^- \to \pi^+\pi^- h_c$ [4]; $(1+\delta^v)$ is the vacuum polarization factor [18]; ϵ_i is the detection efficiency for the ith η_c decay mode in the decay $e^+e^- \to \pi^0\pi^0 h_c$ without consideration of any possible intermediate structures and with ISR and vacuum polarization effects considered in the MC simulation; $\mathcal{B}(\eta_c \to X_i)$ is the corresponding η_c branching fraction; $\mathcal{B}(h_c \to \gamma\eta_c)$ is the branching fraction of $h_c \to \gamma\eta_c$.

The measured Born cross sections are listed in Table I. The ratios of the Born cross sections for the neutral and charged $e^+e^- \to \pi\pi h_c$ modes are also listed in Table I; the cross sections for the charged channel are taken from Ref. [4], where vacuum polarization effects were not taken into account. A corresponding correction factor $(1+\delta^v)$ is applied to the previous Born cross section. The common systematic uncertainties in the two measurements cancel in the ratio calculation. The combined ratio $\mathcal{R}_{\pi\pi h_c}$ is obtained with a weighted least squares method [19] and determined to be (0.63 ± 0.09), which is within 2σ of the expectation of isospin symmetry, 0.5.

Systematic uncertainties in the cross section measurement mainly come from the luminosity measurement ($\delta_{\mathcal{L}}$), branching fraction of $h_c \to \gamma\eta_c$, branching fractions of $\eta_c \to X_i$, detection efficiencies ($\delta_{\epsilon_i \cdot \mathcal{B}(\eta_c \to X_i)}$), radiative correction factors (δ_{ISR}), vacuum polarization factors (δ_{Vac}) [18], and fits to the mass spectrum. The integrated luminosity at each CME points is measured using large-angle Bhabha events and has an estimated uncertainty of 1.0%. The $h_c \to \gamma\eta_c$ and $\eta_c \to X_i$ branching fractions are taken from Refs. [15, 20], and the uncertainties in the radiative correction are the same as those used in the analysis of $e^+e^- \to \pi^+\pi^- h_c$ [4]. The uncertainties in the vacuum polarization factor are 0.5% [18]. The detection efficiency uncertainty estimates are done with the same way as described in Refs. [15, 21]. The uncertainty due to the η_c mass ($\delta_{\eta_c-\mathrm{mass}}$) is estimated by changing its mass by $\pm 1\sigma$ of its world average value [16]; the uncertainties due to the background shapes (δ_{bkg}) are estimated by changing the background function from a first-order to a second-order polynomial; the uncertainty from the mass resolution (δ_{res}) is estimated by varying the mass resolution difference between data and MC simulation by one standard deviation; the uncertainty from fit range (δ_{fit}) is estimated by extending the fit range; the uncertainty from the $\pi^0\pi^0 h_c$ substructure (δ_{sub}) is estimated by considering the efficiency with and without the inclusion of a $Z_c(4020)^0$. The contribution from each source of systematic error are listed in Table II.

Assuming all of the above uncertainties are independent, the total systematic uncertainties in the $e^+e^- \to \pi^0\pi^0 h_c$ cross section measurements are determined to be between 10% and 13%. The uncertainty in $\mathcal{B}(h_c \to \gamma\eta_c)$, not listed in Table II but common to all CME points, is 15.7% [16] and is quoted separately in the cross section measurement.

Intermediate states are studied by examining the $M_{\pi^0}^{\mathrm{recoil}}$ distribution (which corresponds to the reconstructed $\pi^0 h_c$ invariant mass) for the selected $\pi^0\pi^0 h_c$ candidate events. The h_c signal events are selected by requiring 3.51 GeV/c^2 $< M_{\pi^0\pi^0}^{\mathrm{recoil}} <$ 3.55 GeV/c^2, and events in the sideband regions 3.45 GeV/c^2 $< M_{\pi^0\pi^0}^{\mathrm{recoil}} <$ 3.49 GeV/c^2 and 3.57 GeV/c^2 $< M_{\pi^0\pi^0}^{\mathrm{recoil}} <$ 3.61 GeV/c^2 are used to study the background.

TABLE II. The systematic uncertainties (%) in $\sigma^{\mathrm{B}}(e^+e^- \to \pi^0\pi^0 h_c)$.

$\sqrt{s}$ (GeV)	$\delta_{\mathcal{L}}$	δ_{fit}	δ_{res}	δ_{bkg}	$\delta_{\eta_c-\mathrm{mass}}$	δ_{sub}	δ_{ISR}	δ_{Vac}	$\delta_{\epsilon_i \mathcal{B}(\eta_c \to X_i)}$
4.230	1.0	1.3	0.9	5.9	1.6	2.1	2.2	0.5	7.2
4.260	1.0	0.9	0.4	9.5	4.8	1.6	2.3	0.5	7.3
4.360	1.0	1.0	0.1	7.1	4.6	0.6	0.4	0.5	7.2

From the two combinations of the π^0 recoil mass in each event, we retain the one with the larger π^0 recoil mass value, and denote this as $M_{\pi^0}^{\mathrm{recoil}}|_{\mathrm{max}}$. Fig. 2 shows a Dalitz plot of all the $\pi^0\pi^0 h_c$ candidate events summed over the three center-of-mass energies, where there is an evident horizontal band of $M_{\pi^0}^{\mathrm{recoil}}|_{\mathrm{max}}$ values. Figure 3 shows the $M_{\pi^0}^{\mathrm{recoil}}|_{\mathrm{max}}$ distribution for the signal events where there is an obvious peak near 4.02 GeV/c^2, which corresponds to the expected position of a $Z_c(4020)^0$ signal.
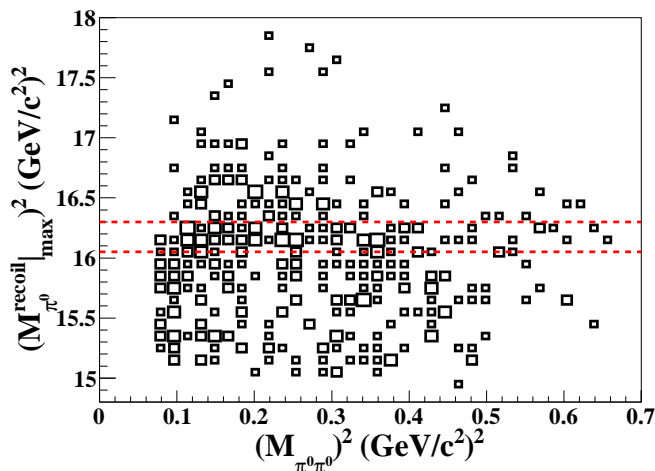

FIG. 2. Dalitz plot of $(M_{\pi^0}^{\mathrm{recoil}}|_{\mathrm{max}})^2$ versus $(M_{\pi^0\pi^0})^2$ for selected $e^+e^- \to \pi^0\pi^0 h_c$ events summed over three CME points. The two red dashed lines represent the potential region of the structure candidates.

An unbinned maximum likelihood fit is applied to the $M_{\pi^0}^{\mathrm{recoil}}|_{\mathrm{max}}$ distribution summed over all 16 η_c decay modes. The data at $\sqrt{s}$ = 4.23, 4.26, and 4.36 GeV are fitted simultaneously with the same signal function with common mass and width. The signal shape is parametrized with a constant-width relativistic Breit-Wigner function convolved with a Gaussian-distributed mass resolution, where the mass resolution is determined from a fit to a MC sample with the width set to zero. Because of the limited statistics of the $Z_c(4020)^0$ signal, its width is fixed to that of its charged partner, (7.9 ± 2.6) MeV [4]. Assuming the spin and parity of the $Z_c(4020)^0$ are 1^+, a phase space factor pq^3 is included in the partial width, where p is the $Z_c(4020)^0$ momentum in the e^+e^- rest frame and q is the h_c momentum in the $Z_c(4020)^0$ rest frame.
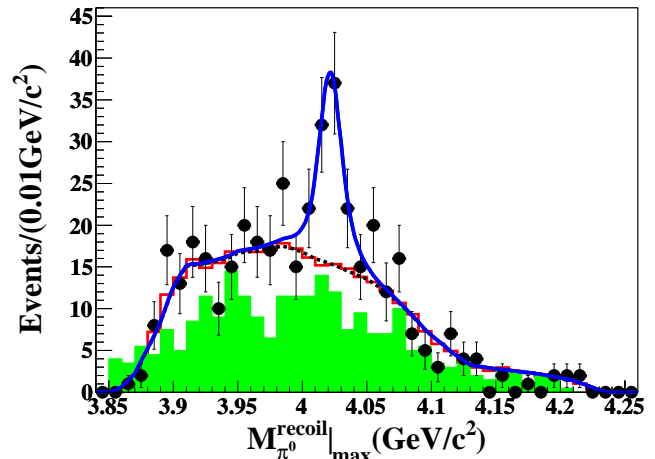

FIG. 3. Sum of the simultaneous fit to the $M_{\pi^0}^{\mathrm{recoil}}|_{\mathrm{max}}$ distribution at $\sqrt{s}$ = 4.23, 4.26 and 4.36 GeV as described in the text. Dots with errors bars are data; the green shaded histogram shows the normalized h_c sideband events; the black dashed curve is the background from the fit; the red histogram shows the result from a phase space MC simulation. The solid blue line shows the total fit.

There are two types of backgrounds in the $M_{\pi^0}^{\mathrm{recoil}}|_{\mathrm{max}}$ distribution. One is the non-h_c background in the h_c signal region, which can be represented by the h_c sideband events, and the other is the non-$Z_c(4020)^0$ $\pi^0\pi^0 h_c$ events that may come from three-body $\pi^0\pi^0 h_c$ decays or from production of intermediate scalar states, such as the $f_0(980)$, that decay into $\pi^0\pi^0$. Since the widths of the low-mass scalar particles are large, these non-$Z_c(4020)^0$ $\pi^0\pi^0 h_c$ events can be reasonably well described with a phase space distribution. For the non-h_c background, a comparison of the h_c sideband events with the simulated phase space events indicates that it can also be described with a three-body phase space distribution. Thus, in the fit all of the background sources are described with a single MC-simulated phase space shape with a total normalization that is left as a free parameter. In the fit, the signal shape mentioned above is multiplied by the efficiency which depends on $M_{\pi^0}^{\mathrm{recoil}}|_{\mathrm{max}}$, but possible interference between the signal and background is neglected.

The solid curve in Fig. 3 shows the fit results, which yields a $Z_c(4020)^0$ mass of 4023.9 ± 2.2 MeV/c^2. By projecting the events into a histogram with 50 bins, the goodness of the fit is calculated from the combined χ^2

values, the number of bins and the number of free parameters at three CME points, and found to be $\chi^2/n.d.f. = 28.6/33$. Here the event number in each bin used in the χ^2 evaluation is required to be larger than 7. The statistical significance of the $Z_c(4020)^0$ signal is determined from a comparison of the fit likelihoods with and without the signal. Additional fit are also performed with different signal shapes, and background shapes. In all cases, the minimum significance is found to be above 5σ. The numbers of $Z_c(4020)^0$ signal events are listed in Table III.

The Born cross section $\sigma^B(e^+e^- \to \pi^0 Z_c(4020)^0 \to \pi^0\pi^0 h_c)$ is calculated with eq. 1, with the measured numbers of observed signal and MC-determined detection efficiencies for the $\pi^0 Z_c(4020)^0$ channel.

The systematic uncertainties on the $Z_c(4020)^0$ mass come from uncertainties in the mass calibration and energy scale, parametrizations of the signal and background shapes, mass dependence of the efficiency, width assumption, MC modeling with a different J^P value, and mass resolution. The uncertainty from the mass calibration is estimated by using the difference, (2.3 ± 1.5) MeV/c^2, between the measured and known h_c mass. The uncertainty from the photon energy scale is estimated with $\psi' \to \gamma\chi_{c1,2}, \chi_{c1,2} \to \gamma J/\psi, J/\psi \to \mu^+\mu^-$ for photons with low energy, and with radiative Bhabha processes for photons with high energy [20]. After adjusting the MC energy scale accordingly, the resulting changes in the mass of $Z_c(4020)^0$ are negligible. The J^P value of $Z_c(4020)^0$ is uncertain; two possible alternatives, $J^P = 1^-$ and 2^+, are used to estimate the corresponding systematic errors. A difference of 0.4 MeV/c^2 in the $Z_c(4020)^0$ mass is found under different J^P assumptions. The uncertainty due to the background shape is determined by changing the phase space shape to a parametrized background function, $f(M) = [(M - M_a)^{1/2} + c_1(M - M_a)^{3/2}] \times [(M_b - M)^{1/2} + c_2(M_b - M)^{3/2}]$. Here M is mass of the background, M_a and M_b are the two extreme points determined by the minimal and maximal mass. $f(M) = 0$ for $(M - M_a) < 0$ or $(M_b - M) < 0$. The coefficients c_1 and c_2 are determined by the fit [10]. A difference of 0.1 MeV/c^2 is found and taken as the systematic uncertainty. The uncertainty due to the mass dependence of the efficiency is determined by assuming a uniform efficiency in the whole $M_{\pi^0}^{\text{recoil}}|_{\text{max}}$ recoil mass region, and the difference is found to be negligible. The uncertainty due to the mass resolution is estimated by varying the data-MC difference in resolution by one standard deviation of the measured uncertainty in the mass resolution of the h_c signal; the difference in the $Z_c(4020)^0$ mass is negligible. Similarly, the uncertainty due to the fixed $Z_c(4020)^0$ width is estimated by varying the width determined for its charged partner by one standard deviation. The difference is 0.1 MeV/c^2 and is taken as the systematic error. Assuming all the sources of the systematic uncertainty are independent, the total systematic error is estimated to be 3.8 MeV/c^2.

The systematic uncertainties in the measured Born cross section, $\sigma(e^+e^- \to \pi^0 Z_c(4020)^0 \to \pi^0\pi^0 h_c)$, are estimated in the same way as for $e^+e^- \to \pi^0\pi^0 h_c$. In addition to those common parts in the $e^+e^- \to \pi^0\pi^0 h_c$ measurement, the uncertainties due to signal parametrization (δ_{signal}), background shape (δ_{bkg}), h_c signal window selection ($\delta_{h_c-\text{signal}}$), mass resolution ($\delta_{\text{res}}$), efficiency ($\delta_{\epsilon_{\text{curve}}}$), and MC model ($\delta_{\text{MC-model}}$) are considered; their values are summarized in Table IV.

The ratios of Born cross section for $e^+e^- \to \pi Z_c(4020) \to \pi\pi h_c$ between neutral and charged modes at three center-of-mass energies are listed in Table III. Similar to the calculation of the $\sigma(e^+e^- \to \pi^0\pi^0 h_c)$ ratio, the same correction factor $(1 + \delta^v)$ is also applied to the previously measured $e^+e^- \to \pi^\pm Z_c(4020)^\mp$ Born cross section. The common systematic uncertainty between neutral and charged mode cancel. The combined ratio $\mathcal{R}_{\pi Z_c(4020)}$ is determined to be (0.99 ± 0.31) with the same method as for the combined $\mathcal{R}_{\pi\pi h_c}$, which is within 1σ of the expectation of isospin symmetry, 1.0.

In summary, we observe $e^+e^- \to \pi^0\pi^0 h_c$ at $\sqrt{s} = 4.23$, 4.26, and 4.36 GeV for the first time. The measured Born cross sections are about half of those for $e^+e^- \to \pi^+\pi^- h_c$, and agree with expectations based on isospin symmetry within systematic uncertainties. A narrow structure with a mass of $(4023.9\pm2.2\pm3.8)$ MeV/c^2 is observed in the $M_{\pi^0}^{\text{recoil}}|_{\text{max}}$ mass spectrum. This structure is most likely the neutral isospin partner of the charged $Z_c(4020)$ observed in the $e^+e^- \to \pi^+\pi^- h_c$ process [4]. This observations indicate that there is no anomalously large isospin violations in $\pi\pi h_c$ and $\pi Z_c(4020)$ system.

TABLE III. Energies ($\sqrt{s}$), numbers of events ($n^{\mathrm{obs}}_{Z_c(4020)^0}$), average efficiencies ($\sum\limits_{i=1}^{16} \epsilon_i \mathcal{B}(\eta_c \to X_i)$), initial state radiative correction factor ($1 + \delta^r$) [4], vacuum polarization factor ($1 + \delta^v$), Born cross sections $\sigma(e^+e^- \to \pi^0 Z_c(4020)^0 \to \pi^0\pi^0 h_c)$, and ratios $\mathcal{R}_{\pi Z_c(4020)} = \frac{\sigma(e^+e^- \to \pi^0 Z_c(4020)^0 \to \pi^0\pi^0 h_c)}{\sigma(e^+e^- \to \pi^\pm Z_c(4020)^\mp \to \pi^\pm\pi^\mp h_c)}$, where the third errors are from the uncertainty in $\mathcal{B}(h_c \to \gamma\eta_c)$ [15].

$\sqrt{s}$ (GeV)	$n^{\mathrm{obs}}_{Z_c(4020)^0}$	$(1+\delta^r)$	$1+\delta^v$	$\sum\limits_{i=1}^{16} \epsilon_i \mathcal{B}(\eta_c \to X_i)$	$\sigma^{\mathrm{B}}(e^+e^- \to \pi^0 Z_c(4020)^0 \to \pi^0\pi^0 h_c)$ (pb)	$R_{\pi Z_c(4020)}$
4.230	21.7 ± 7.4	0.756	1.056	7.08×10^{-3}	$6.5 \pm 2.2 \pm 0.7 \pm 1.0$	$0.77 \pm 0.31 \pm 0.25$
4.260	22.5 ± 7.7	0.831	1.054	6.72×10^{-3}	$8.5 \pm 2.9 \pm 1.1 \pm 1.3$	$1.21 \pm 0.50 \pm 0.38$
4.360	17.2 ± 7.2	0.856	1.051	6.56×10^{-3}	$9.9 \pm 4.1 \pm 1.3 \pm 1.5$	$1.00 \pm 0.48 \pm 0.32$

TABLE IV. Systematic uncertainties (%) in the $\sigma(e^+e^- \to \pi^0 Z_c(4020)^0 \to \pi^0\pi^0 h_c)$ measurement, in addition to part of those in $\sigma(e^+e^- \to \pi^0\pi^0 h_c)$.

$\sqrt{s}$ (GeV)	δ_{signal}	δ_{bkg}	δ_{res}	$\delta_{h_c-\mathrm{signal}}$	$\delta_{\epsilon_{\mathrm{curve}}}$	$\delta_{\mathrm{MC-model}}$
4.230	0.3	5.8	0.5	5.1	0.3	0.6
4.260	1.1	3.5	0.2	8.6	0.3	0.6
4.360	0.8	4.8	0.2	3.5	0.0	0.6

[1] M. Ablikim *et al.* (BESIII Collaboration), Phys. Rev. Lett. **110**, 252001 (2013).

[2] Z. Q. Liu *et al.* (Belle Collaboration), Phys. Rev. Lett. **110**, 252002 (2013).

[3] T. Xiao, S. Dobbs, A. Tomaradze and K. K. Seth, Phys. Lett. B **727**, 366 (2013).

[4] M. Ablikim *et al.* (BESIII Collaboration), Phys. Rev. Lett. **111**, 242001 (2013).

[5] J. Z. Bai *et al.* (BES Collaboration), Nucl. Instrum. Meth. A **344**, 319 (1994); Nucl. Instrum. Meth. A **458**, 627 (2001).

[6] S. Agostinelli *et al.* (GEANT4 Collaboration), Nucl. Instrum. Meth. A **506**, 250 (2003).

[7] S. Jadach, B.F.L. Ward and Z. Was, Comput. Phys. Commun. **130**, 260 (2000); Phys. Rev. D **63**, 113009 (2001).

[8] Q. Wang, C. Hanhart, and Q. Zhao, Phys. Rev. Lett. **111**, 132003 (2013); F.-K. Guo, C. Hidalgo-Duque, J. Nieves, and M. P. Valderrama, Phys. Rev. D **88**, 054007 (2013); G. Li, Eur. Phys. J. C **73**, 2621 (2013); C.-Y. Cui, Y.-L. Liu, W.-B. Chen, and M.-Q. Huang, Eur. Phys. J. C **73**, 12 (2013); J.-R. Zhang, Phys. Rev. D **87**, 116004 (2013); J.M. Dias, F. S. Navarra, M. Nielsen, and C. M. Zanetti, Phys. Rev. D **88**, 016004 (2013); M.B. Voloshin, Phys. Rev. D **87**, 091501 (2013); E. Braaten, Phys. Rev. Lett. **111**, 162003 (2013); E. Wilbring, H.W. Hammer, and U. G. Meißner, Phys. Lett. B **726**, 326 (2013); D.-Y. Chen, X. Liu, and T. Matsuki, Phys. Rev. D **88**, 036008 (2013); K. Terasaki, arXiv:1304.7080; Y.-R. Liu, Phys. Rev. D **88**, 074008 (2013); Q. Wang, C. Hanhart, and Q. Zhao, Phys. Lett. B **725**, 106 (2013); Y. Dong, A. Faessler, T. Gutsche and V. E. Lyubovitskij, Phys. Rev. D **88**, 014030 (2013); X.-H. Liu and G. Li, Phys. Rev. D **88**, 014013 (2013); S. Prelovsek and L. Leskovec, Phys. Lett. B **727**, 172 (2013).

[9] M. Ablikim *et al.* (BESIII Collaboration), Phys. Rev. Lett. **112**, 132001 (2014).

[10] M. Ablikim *et al.* (BESIII Collaboration), Phys. Rev. Lett. **112**, 022001 (2014).

[11] S. K. Choi *et al.* (Belle Collaboration), Phys. Rev. Lett. **100**, 142001 (2008).

[12] K. Chilikin *et al.* (Belle Collaboration), Phys. Rev. D **88**, 074026 (2013).

[13] R. Aaij *et al.* (LHCb Collaboration), Phys. Rev. Lett. **112**, 022002 (2014).

[14] A. Bondar *et al.* (Belle Collaboration), Phys. Rev. Lett. **108**, 122001 (2012).

[15] M. Ablikim *et al.* (BESIII Collaboration), Phys. Rev. D **86**, 092009 (2012).

[16] J. Beringer *et al.* (Particle Data Group), Phys. Rev. D **86**, 010001 (2012).

[17] A track parameter correction procedure [21] is applied to the MC simulated charged tracks to improve the agreement between the data and MC simulation of the χ^2_{4C} distribution of the kinematic fit. The correction factors are obtained from a high purity control sample $J/\psi \to \phi f_0(980)$ with $\phi \to K^+K^-$ and $f_0(980) \to \pi^+\pi^-$. Reasonable agreement between the data and MC simulation is observed for the channels analyzed in this work. The systematic error of the χ^2_{4C} requirement is taken as half of the correction in the efficiency, which is much larger than the effect due to the uncertainties in the correction factors.

[18] S. Actis *et al.*, Eur. Phys. J. C **66**, 585 (2010).

[19] J. Mandel, The Statistical Analysis of Experimental Data, Dover Publications (1964).

[20] M. Ablikim *et al.* (BESIII Collaboration), Phys. Rev. Lett. **104**, 132002 (2010).

[21] M. Ablikim *et al.* (BESIII Collaboration), Phys. Rev. D **87**, 012002 (2013).